J. Fluid Mech. (1993), *vol.* 249, *pp.* 665–688

Modification of grid-generated turbulence by solid particles

By STEFAN SCHRECK[1] AND STANLEY J. KLEIS[2]

[1] Department of Aerospace Engineering, University of Southern California, OHE 530D, Los Angeles, CA 90089-1451, USA

[2] Department of Mechanical Engineering, University of Houston, TX 77004, USA

(Received 15 August 1989 and in revised form 30 October 1992)

The effects of almost neutrally buoyant plastic particles and heavy glass particles on grid-generated turbulence were studied experimentally in a water flow facility. From measured velocities of both the solid and liquid phases, drag and slip velocities of the particles and energy spectra and dissipation rates of the liquid phase were estimated. A monotonic increase in the dissipation rate of the turbulence energy with particle concentration was observed. The increase in energy dissipation rate for suspensions of glass particles was about twice that of suspensions of plastic particles. The increase in dissipation was larger than that predicted by a simple model based on the slip velocities between the phases. It is speculated that the particles enhance the transfer of energy to smaller eddies extending the dissipation spectrum to smaller scales. Since only part of the high wavenumber end of the energy spectrum could be resolved, this speculation cannot be conclusively demonstrated by the present experimental data. The measured velocity spectra do show that the particles increase the isotropy of the flow field and modify the high wavenumber end of the turbulence energy spectrum.

1. Introduction

The development of laser-Doppler velocimeters (LDV) has allowed numerous experimental studies in solid–liquid and solid–gas two-phase flows over the last 20 years. In spite of the large pool of data accumulated, the interaction of solid particles and a turbulent flow field is still not fully understood. One reason for the lack of understanding is that the various effects of the interaction between the phases often cannot be separated. Particles can affect the productions and the dissipation of turbulent energy, enhance or suppress turbulent transport and modify the spectral distribution of turbulent energy. Depending on the flow field and particle size and density, suppression or enhancement of the turbulence intensity of the carrier phase have been reported. Clearly, there exists a need for well-defined experiments in which the various effects of particle–fluid interaction can be investigated separately.

In this study the liquid–solid two-phase flow downstream of a grid is investigated experimentally. The turbulent flow field created by a grid is nearly homogeneous and isotropic. With the absence of mean shear, production and transport of turbulence energy can be neglected. Since no turbulence energy is produced downstream of the wake region of the grid, the local turbulence energy is a function of the dissipation rate only. Furthermore, relationships for isotropic turbulence can be applied to estimate turbulence quantities.

2. Background

It has been generally accepted that sufficiently high concentrations of particles change the fluid turbulence structure. Hetsroni & Sokolov (1971) measured turbulence spectra on the centreline of an axial-symmetric air-jet seeded with small liquid droplets. They obtained data by hot-wire anemometry which showed attenuation of the turbulence energy at high wavenumbers. This finding is in agreement with theoretical work by Baw & Peskin (1971) who predicted suppression of turbulent energy at high wavenumbers by heavy particles in an isotropic turbulence field. Reduction of turbulence energy was estimated from the rate of work by the drag forces created by the rectilinear motion of the particles. Al Taweel & Landau (1976) used a similar model to estimate the effect of particles on the dissipation of turbulent energy. According to their simulations, the suppression of turbulent energy at high wavenumbers reduces the dissipation of turbulent energy by eddy–eddy interaction. At the same time, additional energy is dissipated by friction between the phases. The net result is a decrease in the dissipation rate. Derevich (1987) presented a system of equations for the velocity spectrum of a gas with particles for the case of uniform isotropic turbulence. The set of equations indicates that the energy spectrum is not affected by particles with density equal to the fluid and particles much denser than the fluid. Computed energy spectra agree with those by Al Taweel & Landau in that the turbulence energy in the equilibrium range is attenuated. But, according to Derevich, the range of very small-scale turbulence in the region of viscous dissipation is extended by the presence of particles. The net result is an increase in the total rate of energy dissipation. Tsuji, Morikawa & Shiomi (1984) conducted LDV measurements of an air–solid two-phase flow in a vertical pipe. Both effects of promotion and suppression of turbulence were observed. Turbulence was increased near the centreline of the pipe and decreased near the wall. The spectral distribution of turbulence energy was not changed by large particles. In the presence of small particles, however, the relative amount of turbulence energy at high wavenumbers was increased. This would indicate an increase in the rate of dissipation of turbulence energy.

The present study was undertaken to isolate the effects of particles on the turbulence energy spectrum and energy dissipation rate in the decaying turbulence field downstream of a grid in an attempt to resolve these seemingly contradicting experimental and theoretical results. Heavy glass particles and almost neutrally buoyant plastic particles with diameters of 0.6 to 0.7 mm and volume concentrations of up to 1.5% were added to the flow. LDV measurements of the velocities of both phases were obtained at several locations downstream of the grid. From the velocity records, energy spectra, energy dissipation rates and drag forces exerted on the particles are estimated.

3. Experimental set-up

The study of the velocity fields of both phases of a solid–liquid two-phase flow is particularly difficult when simultaneous measurements of the two velocity fields are desired at high concentrations of particles. This section describes the experimental facilities used for the present investigation.

3.1. *Flow facility*

The flow facility was a vertical closed-loop water tunnel as shown schematically in figure 1. The water was circulated by a low-pressure high-flow rate centrifugal pump.

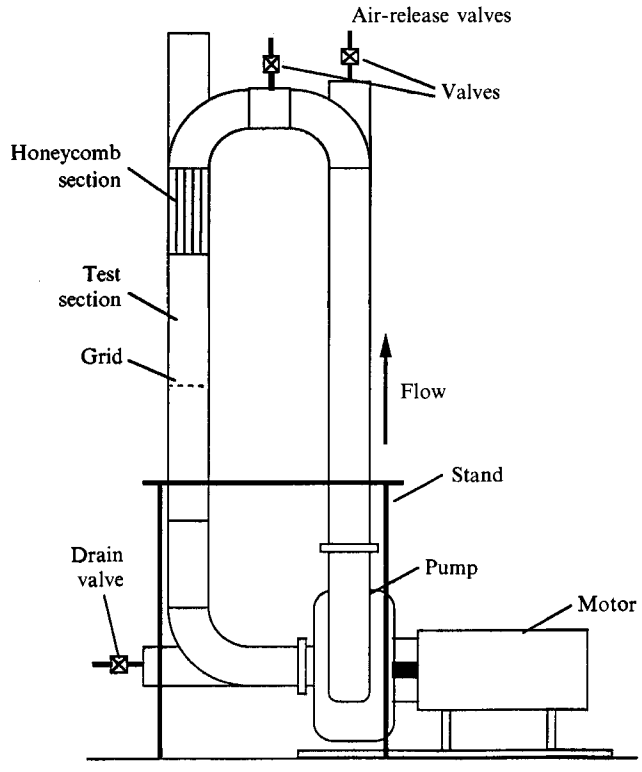

FIGURE 1. Flow facility.

Most parts of the loop of the water tunnel were standard 10.2 cm PVC pipes and fittings. The test section was located in the downward-flowing part of the loop. A series of honeycombs were placed before the inlet of the test section to straighten the flow. The mono-plane grid consisted of square-rods with a grid spacing of $M = 1.78$ cm. The computed solidity ratio was 0.33. The Reynolds number based on the grid size M and the convection velocity $U = 1.0$ m/s was $Re_M = 15600$. Velocity measurements were taken at different locations downstream from the grid. For reasons which are discussed later, the point of measurement in the test section was fixed. Consequently, the grid was moved to take measurements at different locations downstream from the grid. This was achieved by suspending the grid with strings along the wall of the test section. As shown in figure 1, a straight section of PVC pipe was installed vertically above the test section. This section served two purposes. Air bubbles were removed by running the pump at a low speed, allowing the bubbles suspended in the water to rise through this section to the atmosphere. Also, particles were added to and removed from the water through this section.

3.2. *Particles*

Two types of particles were selected for this study: plastic particles with a density of 1045 kg/m^3 and glass particles with a density of 2400 kg/m^3. The particle sizes ranged from 0.60 to 0.71 mm. Both types of particles were selected from large batches of heterogeneously sized particles ranging from 0.025 to 2.0 mm. The size distributions of the selected particles were nearly uniformly distributed between 0.60 and 0.71 mm.

3.3. *Laser-Doppler velocimeter and particle discrimination*

All velocity measurements were conducted with TSI 3-beam 2-component laser Doppler velocimeter. The beams entered the test section coaxial with a tapered cylindrical glass rod having a length of 60 mm. The diameter of the window at the small end of the rod was 5 mm. The sample volume was 20 mm in front of the window in the centre of the test section. The purpose of the rod was to reduce blockage of the beams by particles and to minimize attenuation of Doppler signals. This was considered necessary to maintain a high data rate required for reliable spectral estimates of the velocity fluctuations. LDV measurements were taken in a single-phase flow with the glass rod installed and compared with measurements with the glass rod removed. The measurements showed that the glass rod did not alter the flow field at the point of measurement. TiO_2 particles of size of 2–10 μm were used as tracers for the liquid phase.

To differentiate between signals from the tracer particles and the plastic and glass particles, a combination of amplitude and burst-length discrimination of the Doppler signals was used. The amplitude and burst-length thresholds were determined empirically. To test the discrimination circuit, the facility was first run with only tracer particles in the flow. All Doppler signals were identified by the discrimination circuit as signals from the fluid phase. Secondly, with the fluid at rest and no TiO_2 added to the water, particles were introduced into the facility from the top. Particles passing through the sample volume of the LDV system triggered the discrimination circuit. The associated velocity signals were tagged as particle velocities. On average, 95% of tagged signals were associated with velocities of the order of the settling velocity of the particles. From these results it was concluded that the cross-talk was about 5%. This was considered acceptable for this study.

The data obtained from counter signal processors are random in time. It is well known and discussed in the literature that unweighted averaging of velocity data obtained from counter signal processors can lead to biasing of the results (McLaughlin & Tiederman 1973; Buchhave & George 1979). However, biasing of averaged velocity information can be neglected in low-turbulence gradient-free flow fields such as the one used for this study. Results from velocity statistics using various averaging schemes showed that no difference between weighted and unweighted averages were noticed. Thus, unweighted averaging of the velocity data was used throughout this study. To estimate energy spectra, velocity correlations were computed using the slot method proposed by Buchhave (1979); 100000 points in every slot were needed to achieve a signal-to-noise ratio of about 40 dB.

Difficulties were encountered obtaining reliable estimates for the velocity fluctuations. It was found that the values of the velocity fluctuations estimated by the root mean square (r.m.s.) of the sampled velocity data were dependent on the signal-to-noise ratio of the Doppler burst. The signal-to-noise ratio of the Doppler signals was significantly reduced at high concentration of solid particles. This resulted in an increased uncertainty in the determination of the Doppler frequency by the counter signal processors and, consequently, higher values for the r.m.s. velocities. Since low turbulence intensities of 1% to 5% were expected downstream of the grid, reliable estimates of the velocity fluctuations were crucial for this study. Several data reduction schemes were tested to overcome this problem. Best results were achieved by using a multiple-burst correlation method. The counter signal processors were set to accept bursts of 8 fringe crossings. Particles passing through the centre of the sample volume created multiple bursts. Assuming that the particles do not accelerate during their

transit time, the bursts from one particle carry the same velocity information plus some random uncorrelated noise. By taking the product of two velocity signals from one particle instead of squaring the individual velocity signals, random noise was successfully removed. The new data reduction scheme was tested in the flow facility. Data were taken at a fixed location in the flow field. The signal to noise ratio was varied by changing the focus of the receiving optics. Unlike the r.m.s. method, the multiple-burst correlation method produced consistent estimates of the turbulence intensity.

4. Results

4.1. *Single-phase flow*

The flow field of interest is the core region of the water tunnel from 15 to 33 grid mesh sizes M downstream of the grid. Velocity measurements were taken across the test section to ensure the flow field was free of any wall boundary-layer effects or non-uniformities. Streamwise mean velocities across the test section at station $x = 15\,M$ are shown in figure 2. Streamwise and transverse velocity fluctuations u' and v' at the same location are presented in figure 3. The ratios u'/v' of the streamwise and transverse velocity fluctuations, also shown in figure 3, varied from 1.08 and 1.22. The boundary-layer growth caused a slight increase in the convection velocity in the core region of the water tunnel. The convection velocity measured at the centreline increased by 2.3% from location $x = 15\,M$ to $x = 33\,M$.

The one-dimensional probability densities of the streamwise and transverse velocity components were found to be closely Gaussian. Since the normalized probability distributions along the centreline of the test section were identical within the limit of the uncertainty of the measurements, only a few representative probability densities for u' and v' are plotted in figures 4 and 5, respectively; every curve representing approximately 4 million data.

Figure 6 shows the decay curves for the streamwise and transverse velocity components *vs.* the downstream location x/M. A more rapid decay for the transverse than for the streamwise turbulence intensity is noticed. This is due to the anisotropy of grid-generated turbulence at the large scales. The streamwise velocity component contains more turbulence energy at the large scales. Since the large scales persist longer, they result in an inequality in decay of the streamwise and the transverse velocity components. The ratios u'/v' are presented in figure 7. The values u'/v' range from 1.07 to 1.16. The scattering of the values of u'/v' is of the same order as that observed in grid turbulence in large wind-tunnel facilities (Comte-Bellot & Corrsin 1966). Batchelor & Townsend (1949) proposed the following linear decay law,

$$\frac{U^2}{u^2} = C\frac{x-x_0}{M}, \tag{1}$$

where $3u^2 = u'^2+v'^2+w'^2$, C is the slope of the linear decay law, and x_0 is the location of the virtual origin. The linear decay laws obtained for the two velocity components are:

$$\frac{U^2}{u'^2} = 44.5\left[\frac{x}{M}-6.2\right], \tag{2}$$

$$\frac{U'^2}{v'^2} = 58.1\left[\frac{x}{M}-7.0\right]. \tag{3}$$

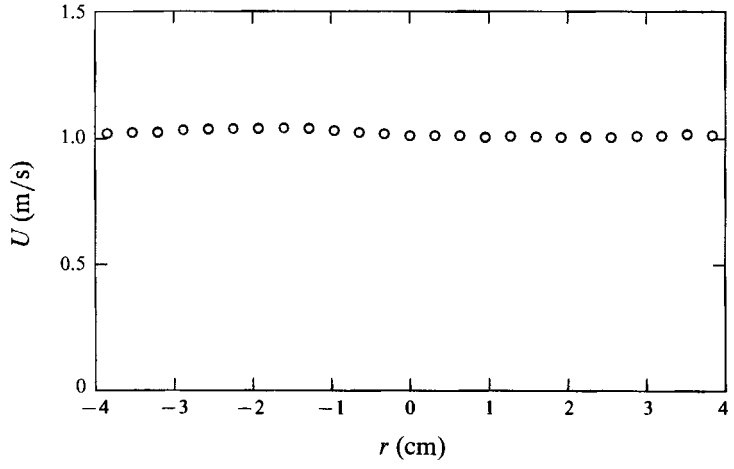

FIGURE 2. Mean velocity profile across the test section at $x/M = 15$.

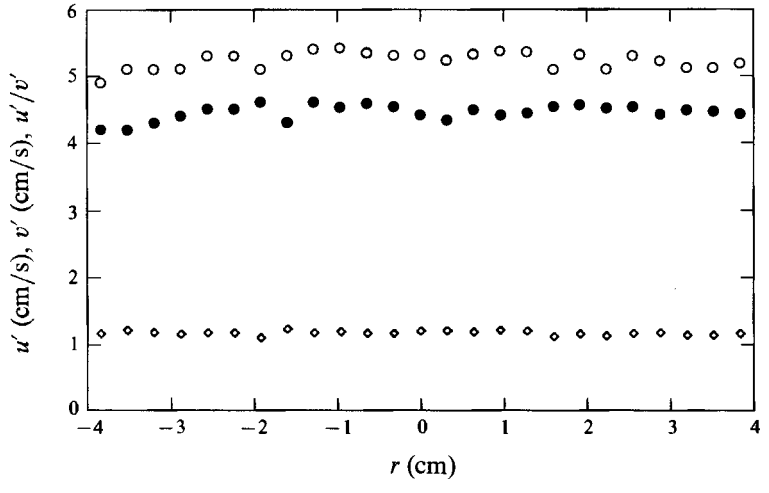

FIGURE 3. Streamwise and transverse velocity fluctuations at $x/M = 15$. ○, u'; ●, v'; ◇, u'/v'.

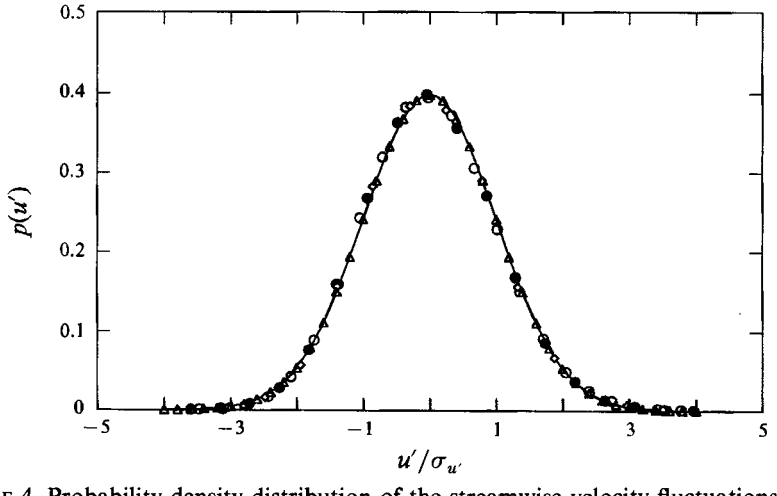

FIGURE 4. Probability density distribution of the streamwise velocity fluctuations for the single-phase flow. ○, $x/M = 15$; ●, $x/M = 22$; ◇, $x/M = 33$.

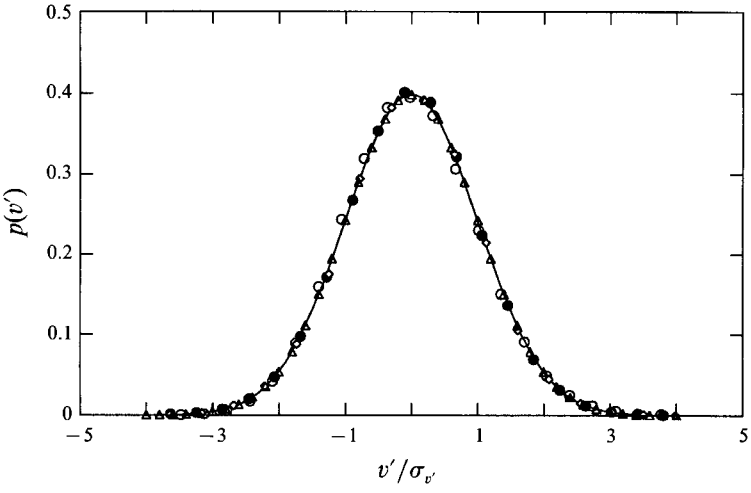

FIGURE 5. Probability density distribution of the transverse velocity fluctuations for the single-phase flow. ○, $x/M = 15$; ●, $x/M = 22$; ◇, $x/M = 33$.

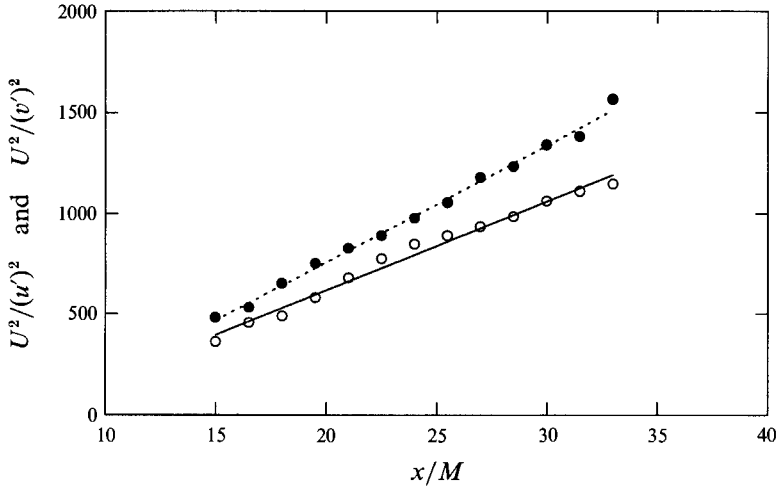

FIGURE 6. Decay curves of the velocity fluctuations u' and v'. —○—, $U^2/(u')^2$; --○--, $U^2/(v')^2$.

Combining the data sets of u' and v', a universal decay law was obtained as follows (figure 8),

$$\frac{U^2}{u^2} = 52.8\left[\frac{x}{M} - 6.7\right]. \tag{4}$$

For derivations of quantities which require the decay law, (4) will be used.

Other important quantities characterizing the turbulent flow field were computed from the decay law. The dissipation rate $\epsilon(t)$ is given by

$$\epsilon(t) = -\frac{3\mathrm{d}}{2\mathrm{d}t}(u^2). \tag{5}$$

With the transformation $\mathrm{d}/\mathrm{d}t = U(\mathrm{d}/\mathrm{d}x)$,

$$\epsilon = -\tfrac{3}{2}U\frac{\mathrm{d}}{\mathrm{d}x}(u^2), \tag{6}$$

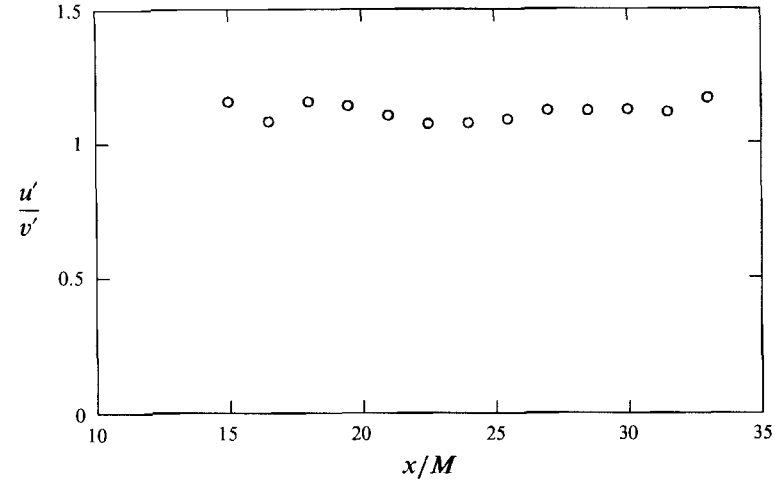

FIGURE 7. Ratio of the velocity fluctuations u'/v'.

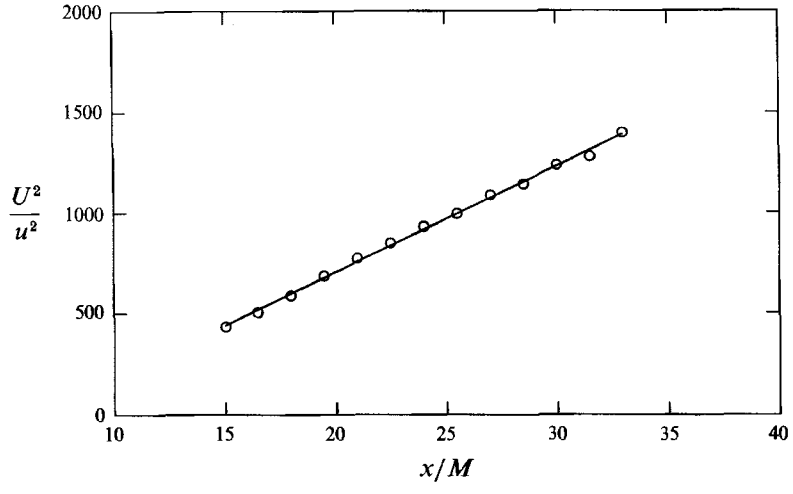

FIGURE 8. Decay curves of the turbulence intensity.

and substituting (1) into (6) yields

$$\epsilon = \frac{3}{2}\frac{U^3}{CM}\left[\frac{x-x_0}{M}\right]^{-2}. \tag{7}$$

For isotropic turbulence, the Taylor microscale λ, the characteristic lengthscale associated with the strain rate fluctuations s_{ij}, is defined as (Hinze 1975)

$$\epsilon = 15\nu\frac{u^2}{\lambda^2}. \tag{8}$$

where ν is the kinematic viscosity of the fluid. Substituting the relationships for u^2 and ϵ into (8),

$$\lambda^2 = 10\nu\frac{M}{U}\left[\frac{x-x_0}{M}\right]. \tag{9}$$

From the dissipation rate ϵ, the Kolmogorov time, length, and velocity microscales were calculated from their definitions.

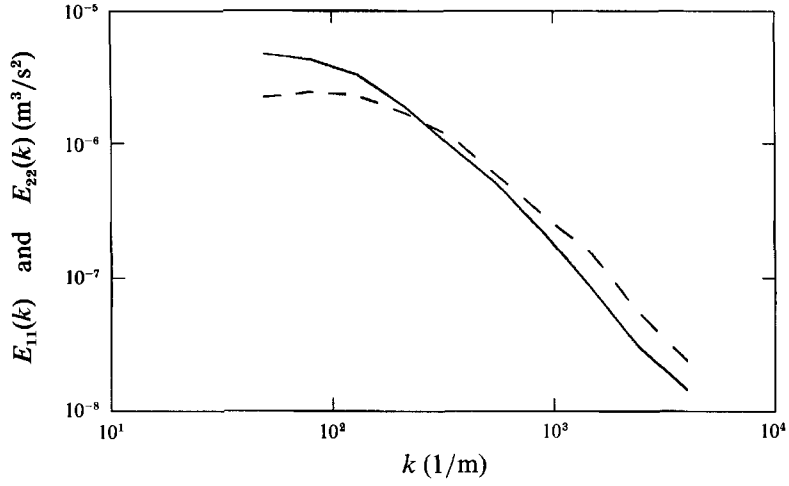

FIGURE 9. Streamwise and transverse energy spectra at $x/M = 22$. —, $E_{11}(k)$; ---, $E_{22}(k)$.

x/M	15	18	22	27	33
U (m/s)	1.001	1.006	1.016	1.022	1.021
u'/U (%)	5.28	4.51	3.76	3.27	1.97
v'/U [%]	4.59	3.92	3.35	2.91	2.54
u/U [%]	4.80	4.12	3.48	3.03	2.68
λ [cm]	0.159	0.185	0.216	0.248	0.283
ϵ [cm^2/s^3]	234	125	68	39	23
η [cm]	0.009	0.011	0.013	0.015	0.016
u_k [cm/s]	1.27	1.09	0.94	0.81	0.70
τ_k [ms]	10.6	14.6	19.9	26.7	34.5

TABLE 1. Turbulence quantities for the single-phase flow

Measured and computed fluid-turbulence quantities for the locations $x/M = 15$, 18, 22, 27 and 33 are listed in table 1. The Reynolds number Re_λ based on the Taylor microscale λ, the r.m.s. velocity u, and the viscosity ν is independent of x as implied by (9) for λ^2 and (1) for u^2,

$$Re_\lambda = \left[\frac{10UM}{C\nu}\right]^{\frac{1}{2}}. \tag{10}$$

The computed value for Re_λ is 65.

From measured autocorrelation functions, the spectral distribution of the turbulence energy was estimated. The longitudinal energy spectrum $E_{11}(k)$ and the lateral energy spectrum $E_{22}(k)$ at $x/M = 22$ are shown in figure 9. The smallest structure which could be resolved by the LDV system was limited to about 0.5 mm. The computed value for the Kolmogorov microscale at $x/M = 22$ is $\eta = 0.14$ mm. Thus, the dissipative end of the equilibrium range could not be fully resolved. At small wavenumbers k, the energy of the streamwise velocity fluctuations is significantly higher than that of the transverse velocity fluctuations. The curves for the two velocity components cross over at $k = 200$ m^{-1}. At large wavenumbers the curve of the transverse velocity component stays higher than that of the streamwise velocity component. This is consistent with hot-wire measurements by Van Atta & Chen (1970).

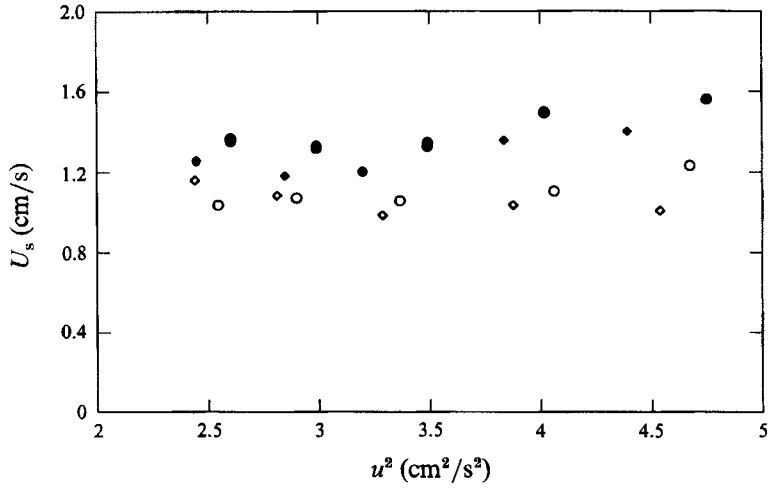

FIGURE 10. Settling velocities of plastic particles as a function of the turbulence intensity. ●, $C = 0.4\%$; ○, $C = 0.8\%$; ◆, $C = 1.2\%$; ◇, $C = 1.5\%$.

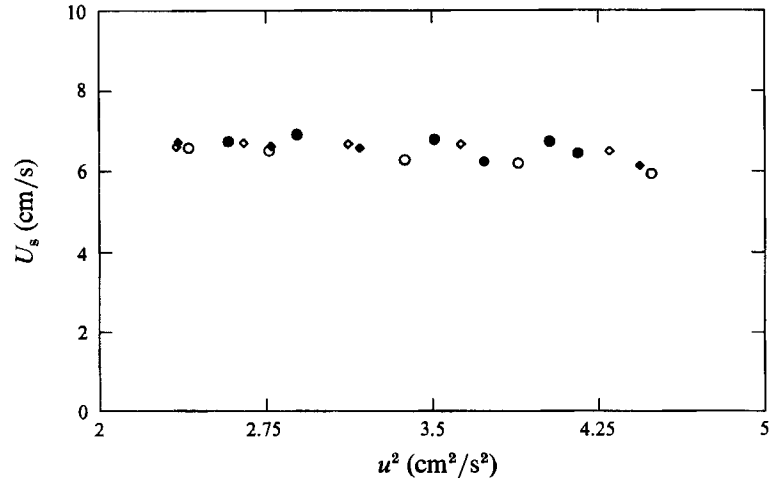

FIGURE 11. Settling velocities of glass particles as a function of the turbulence intensity. ●, $C = 0.4\%$; ○, $C = 0.8\%$; ◆, $C = 1.2\%$; ◇, $C = 1.5\%$.

The obtained results establish the basic flow field as a typical single-phase grid turbulence flow and define the range of turbulence scales which could be resolved.

4.2. *Particle motion*

To the basic flow field, plastic and glass particles were added in volume concentrations of 0.4, 0.8, 1.2 and 1.5%. Since the particles were recirculated and passed through the grid, some particles might strike the grid and become deflected. Based on the average relaxation time of the particles ($\tau = 38$ and 69 ms for the plastic and glass particles, respectively), particles were expected to have recovered from any contact with the grid before they reach the first point of measurement about 270 ms after passing through the grid.

Particle and fluid velocities were measured along the centreline of the test section at $x/M = 15$, 18, 22, 27 and 33. Figures 10 and 11 show the measured particle settling velocities as a function of the turbulence level of the liquid phase. The settling velocities

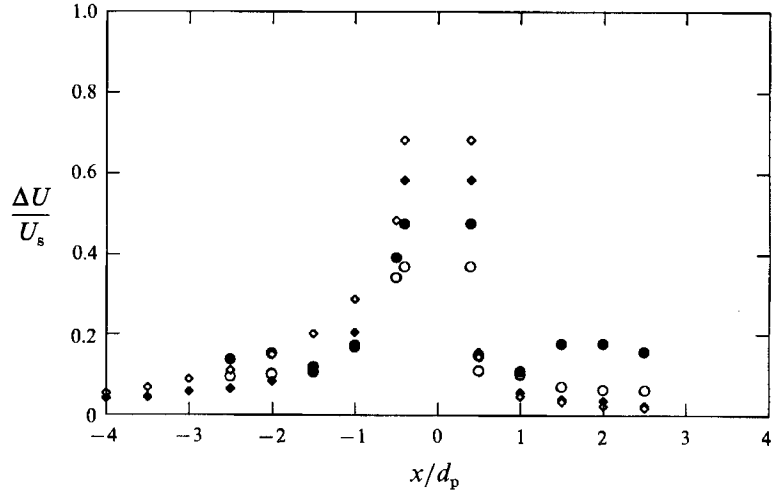

FIGURE 12. Streamwise velocity profiles of the boundary layer of the particles. Plastic particles: ●, at $x/M = 15$; ○, at $x/M = 33$. Glass particles: ◆, at $x/M = 15$; ◇, at $x/M = 33$.

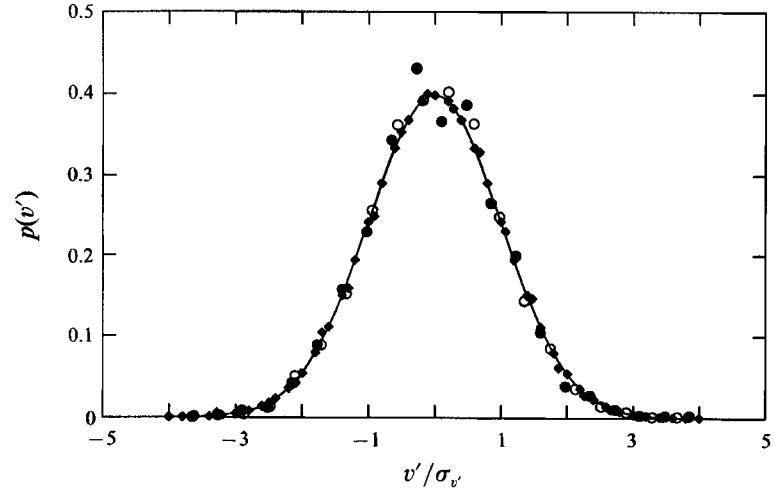

FIGURE 13. Probability density distribution of the transverse velocity fluctuations of plastic particles at $x/M = 22$. ●, $C = 0.4\%$; ○, C = 0.8%; ◆, $C = 1.5\%$.

were estimated by subtracting the mean velocity of the fluid from the mean velocity of the particles. The average settling velocity of the plastic particles was 1.25 cm/s, the average settling velocity of the glass particles was 6.40 cm/s. The uncertainty in the data is about 0.1 cm/s. The settling velocities are independent of the turbulence intensity over the range of intensities studied. The computed Reynolds numbers of the particles based on their diameter and their average settling velocities are $Re_d = 8$ for plastic particles and $Re_d = 39$ for glass particles. The computed drag coefficient is about $C_D = 3$ for both glass and plastic particles.

Velocity signals of the fluid were conditionally sampled and phase averaged with respect to the centre of the particles. Resulting mean velocity profiles in the vicinity of the particles are shown in figure 12. The local free-stream velocity is subtracted from the measured velocities and the resulting velocity difference is normalized by the

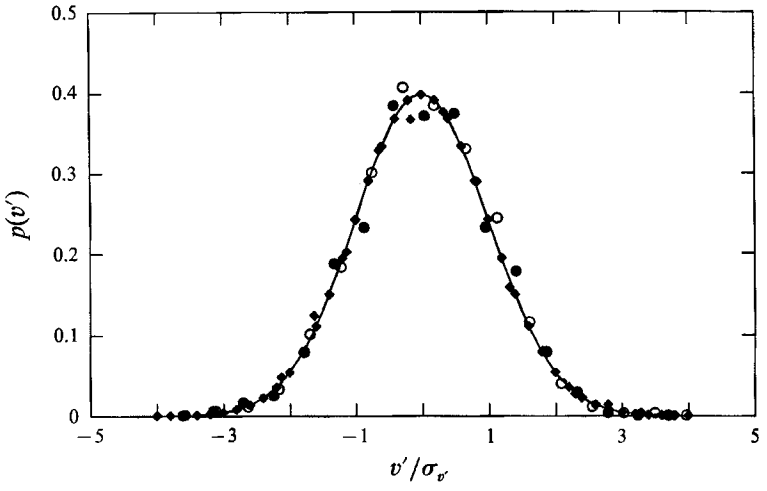

FIGURE 14. Probability density distribution of the transverse velocity fluctuations of glass particles at $x/M = 22$. ●, $C = 0.4\%$; ○, $C = 0.8\%$; ◆, $C = 1.5\%$.

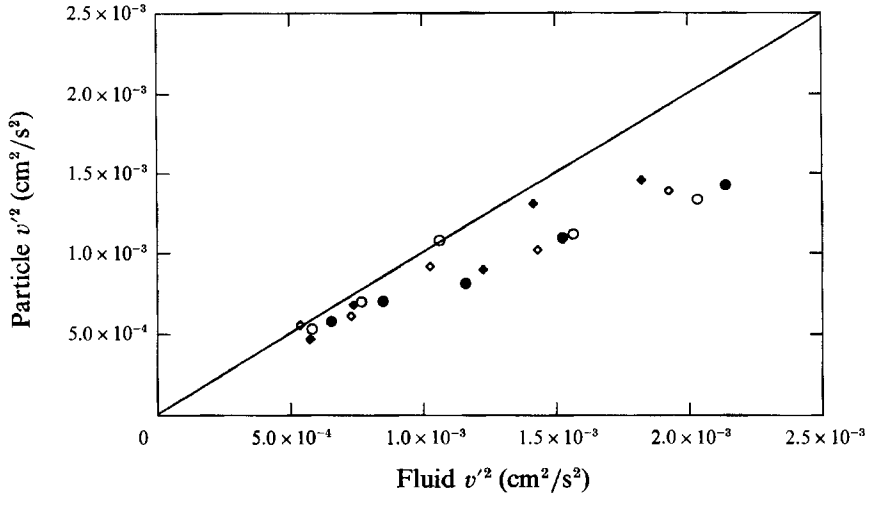

FIGURE 15. Transverse mean square velocity fluctuations of plastic particles as a function of the transverse mean square velocity fluctuations of the fluid. ●, $C = 0.4\%$; ○, $C = 0.8\%$; ◆, $C = 1.2\%$; ◇, $C = 1.5\%$.

settling velocities U_S. The streamwise distance, x, is normalized by the particle diameter d_p. Locations in the wake of the particles are indicated by positive values of x/d_p. The shape of the boundary layers around the plastic and the glass particles are similar. The skewed velocity profiles indicate the formation of wakes behind the particles.

In figures 13 and 14, the probability density distributions of the transverse velocity components of plastic and glass particles are presented. Each set of data represents about 3000 to 4000 particles. The probability density distributions are closely Gaussian. Figures 15 and 16 show the mean square of the transverse velocity fluctuations for the plastic and glass particles versus the mean square of the velocity fluctuations of the fluid. The line $(U_p/U_f)^2 = 1$ is shown for reference. The uncertainty in the mean square velocities of the particles is about 10% and that of the fluid about

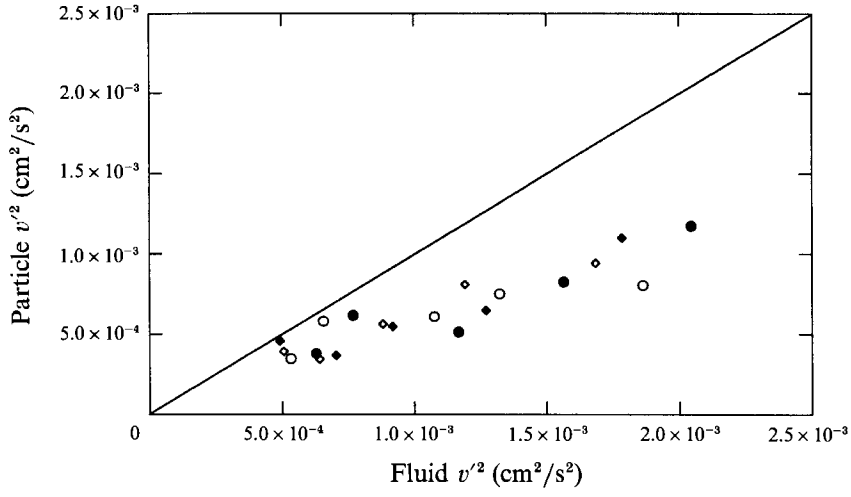

FIGURE 16. Transverse mean square velocity fluctuations of glass particles as a function of the transverse mean square velocity fluctuations of the fluid. ●, $C = 0.4\%$; ○, $C = 0.8\%$; ◆, $C = 1.2\%$; ◇, $C = 1.5\%$.

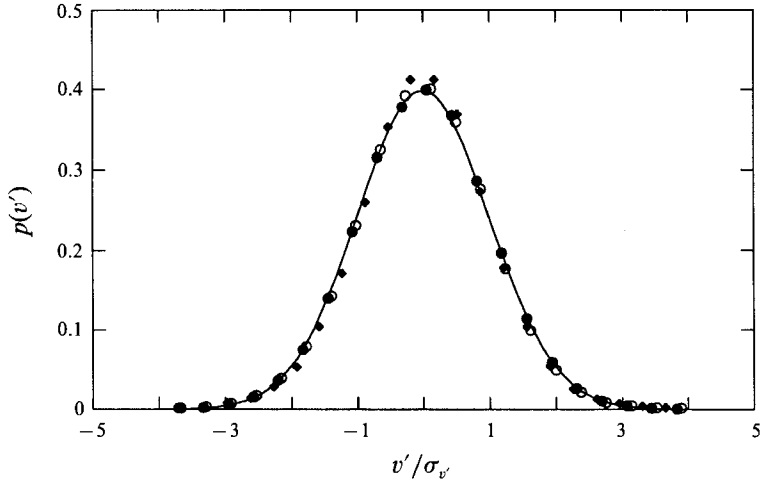

FIGURE 17. Probability density distribution of the transverse velocity fluctuations of the liquid phase in the suspensions of plastic particles. ●, $C = 0.4\%$; ○, $C = 0.8\%$; ◆, $C = 1.5\%$.

5%. The difference between the particle and the fluid velocity fluctuations increases with turbulence intensity. This trend is more apparent in the case of the heavier glass particles than in the case of the almost neutrally buoyant plastic particles. No trend with concentration is evident.

4.3. *Turbulence of the suspensions*

The effects of particles on the structure of the turbulence field downstream of the grid were investigated for particle volume concentrations of 0.4% to 1.5%. For concentrations less than 0.4%, the rate of occurrence of velocity signals from particles is too low to acquire sufficient data for statistical averages in a reasonable period of

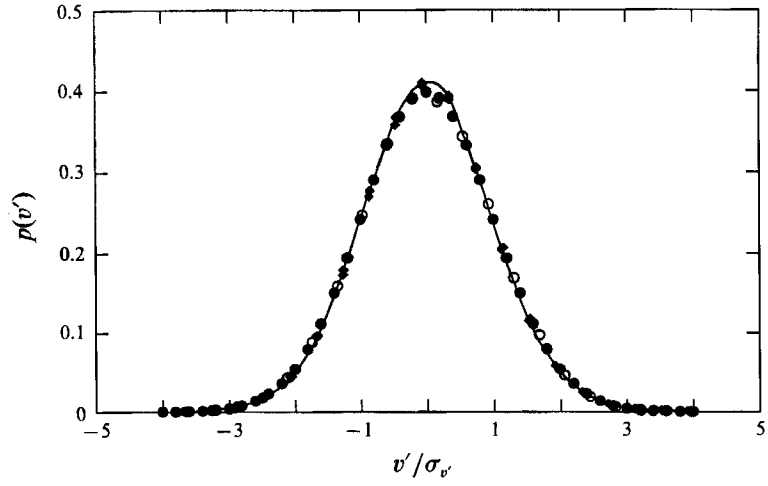

FIGURE 18. Probability density distribution of the transverse velocity fluctuations of the liquid phase in the suspension of glass particles, ●, $C = 0.4\%$; ○, $C = 0.8\%$; ◆, $C = 1.5\%$.

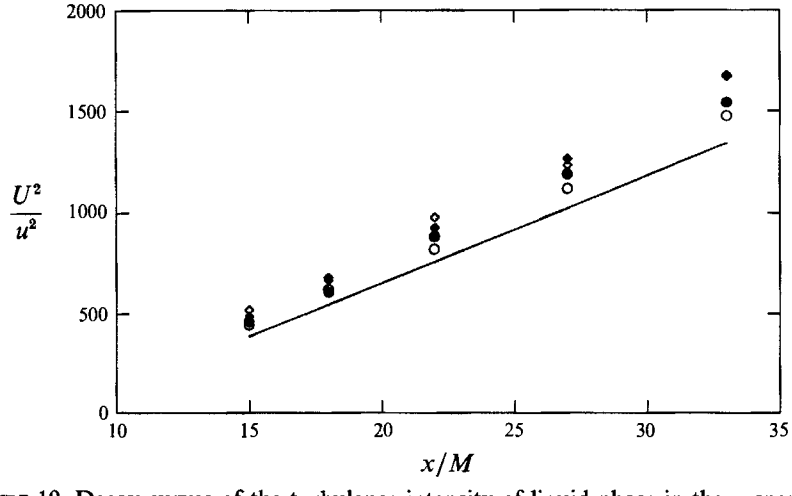

FIGURE 19. Decay curves of the turbulence intensity of liquid phase in the suspension of plastic particles. —, 0%; ○, 0.4%; ●, 0.8%; ◇, 1.2%; ◆, 1.5%.

time. At concentrations of more than 1.5%, instabilities in the flow were observed. These instabilities were of low frequencies, presumably caused by particles moving in groups resulting in a large-scale fluctuation of the particle concentration. Velocity statistics would have been strongly affected by these low-frequency instabilities. Figures 17 and 18 show probability density distributions of the transverse velocity components of the fluid at $x/M = 22$ for different particle concentrations. The probability density distributions did not change with particles added to the flow, i.e. the distributions remain closely Gaussian.

In figures 19 and 20, the decay curves for the liquid phase in the two suspensions are presented. The decay law of the single-phase flow is indicated by the straight lines. The turbulence intensity is monotonically decreased with increasing concentration of particles. For each volume concentration, the velocity fluctuations for the suspensions

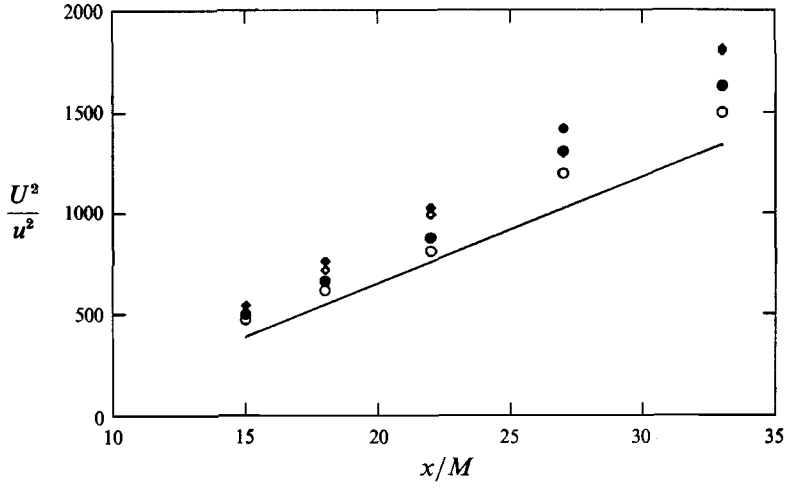

FIGURE 20. Decay curves of the turbulence intensity of the liquid phase in the suspension of glass particles. —, 0%; ○, 0.4%; ●, 0.8%; ◇, 1.2%; ◆, 1.5%.

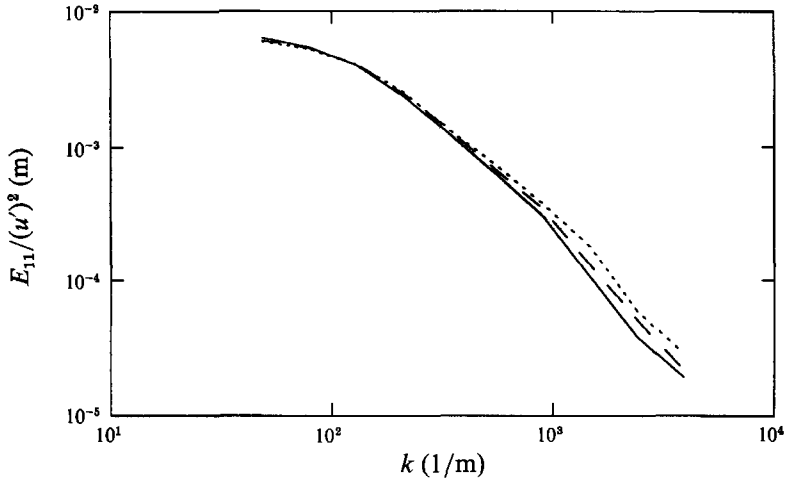

FIGURE 21. Streamwise energy spectra of the liquid phase in the suspension of plastic particles at $x/M = 22$. —, 0%; ——, 0.8%; · · ·, 1.5%.

of glass particles are lower than that of the suspensions of plastic particles. The steeper slopes of the decay curves for the suspensions indicate an increase in the dissipation rate.

At the location $x/M = 22$, energy spectra were computed from measured auto-correlations of the fluid velocities. Longitudinal and transverse energy spectra are presented in figures 21 to 24. The data were smoothed by averaging the spectral values over one-third of a decade. The presence of particles slightly increases the energy at the high wavenumber end of the longitudinal spectra. This is more noticeable in the case of plastic particles than in the case of glass particles. The effect of particles on the transverse spectra is the opposite; the energy at high wavenumbers stays the same or is slightly reduced. When the longitudinal and transverse spectra are plotted together (figures 25 and 26), an increase in the isotropy at high wavenumbers compared to the

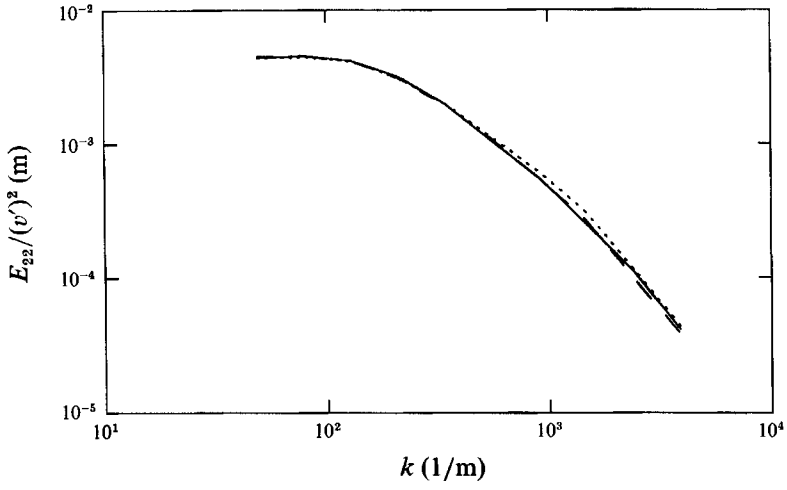

FIGURE 22. Transverse energy spectra of the liquid phase in the suspension of plastic particles at $x/M = 22$. —, 0%; – – –, 0.8%; · · ·, 1.5%.

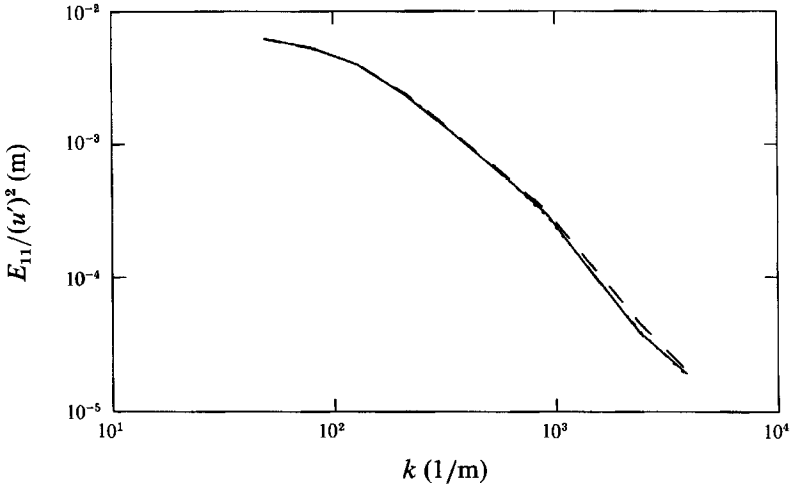

FIGURE 23. Streamwise energy spectra of the liquid phase in the suspension of glass particles at $x/M = 22$. —, 0%; – – –, 0.8%; · · ·, 1.5%.

single-phase flow is noticed. From the spectra $E_{11}(k)$ and $E_{22}(k)$, the one-dimensional spectrum $E_{ii}(k)$ was computed. Assuming that $E_{33}(k)$ equals $E_{22}(k)$, $E_{ii}(k)$ was estimated by

$$E_{ii}(k) = E_{11}(k) + 2E_{22}(k), \tag{11}$$

Figures 27 and 28 show one-dimensional energy spectra $E_{ii}(k)$ for the liquid phase in suspensions of plastic and glass particles together with that of the single-phase flow. The opposing effects of the particles on the longitudinal and transverse spectra result in only small changes in the distribution of the total energy. In the case of plastic particles, the energy at high wavenumbers seems to be almost unchanged, while that of the glass particles is slightly reduced. However, the observed differences are of the order of the uncertainty in the data.

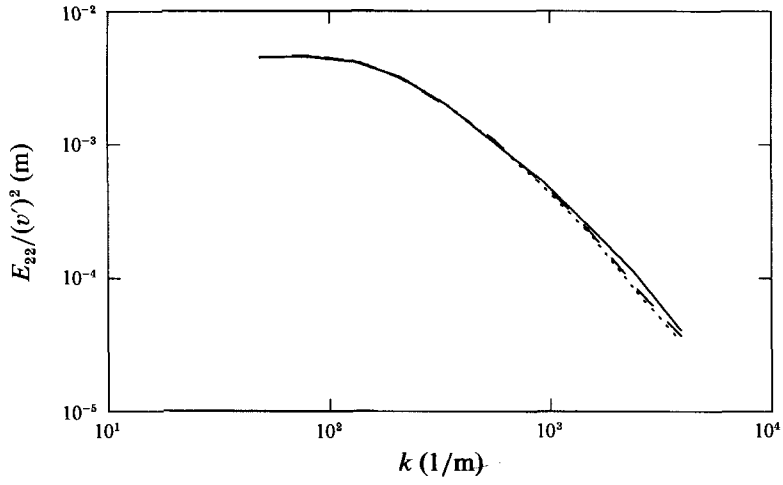

FIGURE 24. Transverse energy spectra of the liquid phase in the suspension of glass particles at $x/M = 22$. —, 0%; – – –, 0.8%; · · ·, 1.5%.

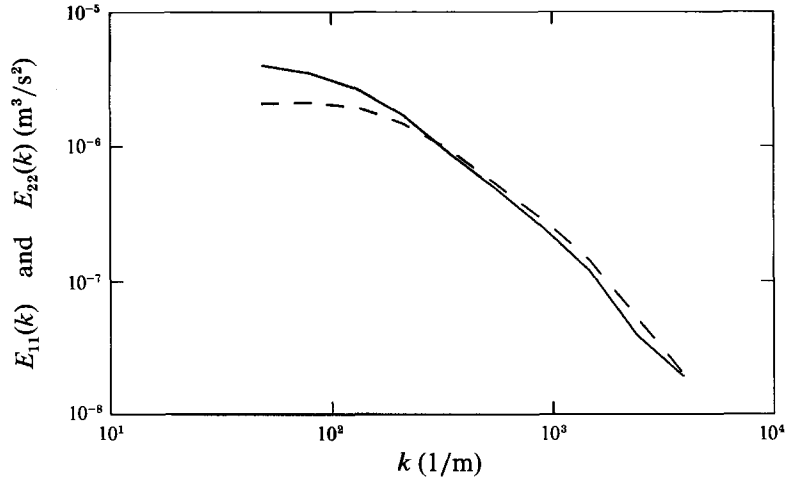

FIGURE 25. Streamwise and transverse energy spectra of the liquid phase in the suspension of plastic particles for a volume concentration of 1.5% at $x/M = 22$. —, $E_{11}(k)$; – – –, $E_{22}(k)$.

5. Discussion

5.1. *Particle motion*

To predict the effect of the particles on the turbulence field, the momentum exchange between the phases was estimated. In most of the theoretical studies, only the drag force due to the rectilinear relative motion between the phases has been considered (Baw & Peskin 1971; Hetsroni & Sokolov 1971; Derevich 1987). Estimates of the drag coefficient are often based on Stokes' law for spheres,

$$c_D = 24/Re. \tag{12}$$

These idealizations are only valid for particles much smaller than the Kolmogorov microscale and for particle Reynolds numbers $Re_d < 1$. The computed Reynolds numbers of the plastic and glass particles are 8 and 39, respectively. The computed drag coefficients for both types of particles is about $c_D = 3$. In the case of the plastic particles

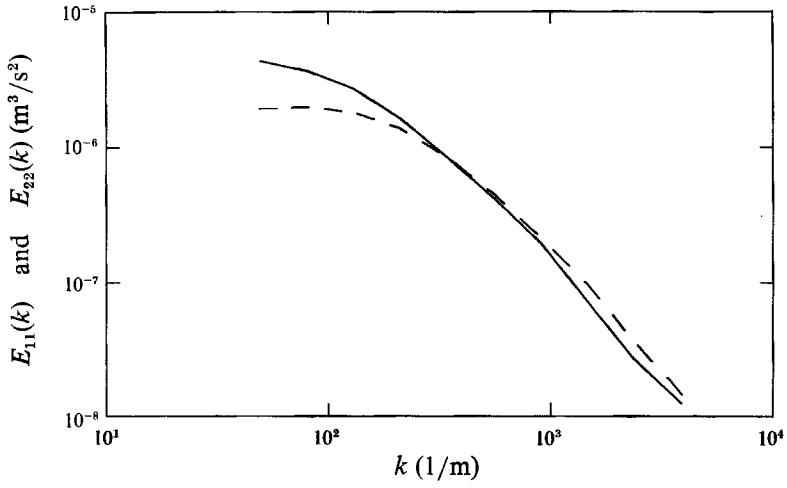

FIGURE 26. Streamwise and transverse energy spectra of the liquid phase in the suspension of glass particles for a volume concentration of 1.5% at $x/M = 22$. —, $E_{11}(k)$; – – –, $E_{22}(k)$.

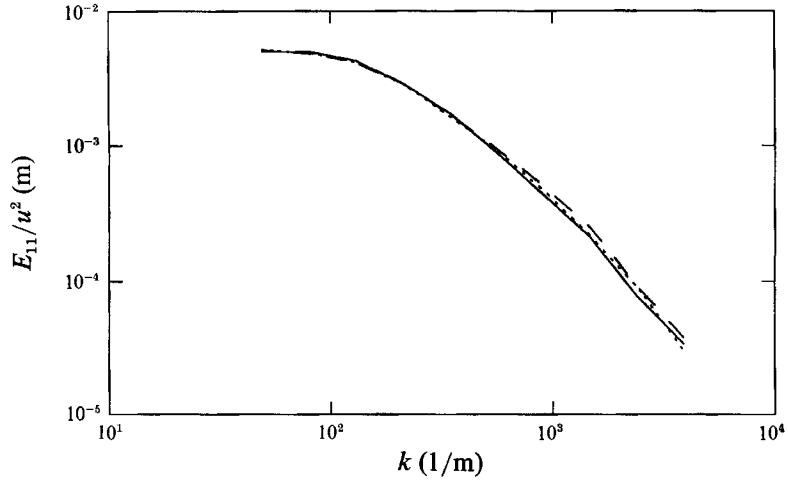

FIGURE 27. One-dimensional energy spectra of the liquid phase in the suspension of plastic particles at $x/M = 22$. —, 0%; · · ·, 0.8%; – – –, 1.5%.

this is in very good agreement with the drag coefficient predicted by (12). This is somewhat surprising considering that the flow field is highly turbulent. However, it is consistent with work by Lee (1987), who studied the settling velocities of solid particles in turbulent gas flows. Lee introduced an apparent turbulence viscosity to predict the settling velocities of solid particles in a turbulent air stream. The ratio of turbulent viscosity to fluid viscosity was correlated with the Froude number, the particle concentration, and the turbulence Reynolds number. According to Lee's model, the apparent turbulence viscosity is equal to the fluid viscosity for particle Reynolds numbers less than 10, i.e. the drag coefficient is described by (12). The model, however, fails to predict the drag coefficient of the glass beads correctly. Lee's prediction is an order of magnitude too high. This might be due to the large differences in the density ratios ρ_p/ρ_f considered by Lee ($\rho_p/\rho_f > 800$) and the present study ($\rho_p/\rho_f < 3$).

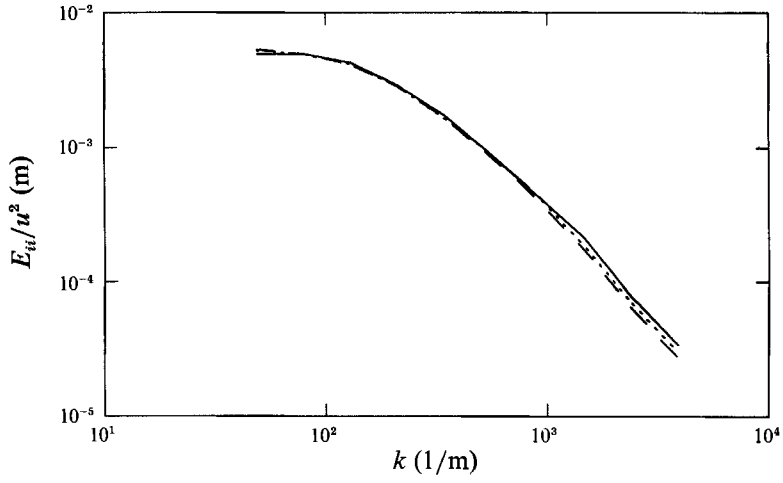

FIGURE 28. One-dimensional energy spectra of the liquid phase in the suspension of glass particles at $x/M = 22$. —, 0%; · · ·, 0.8%.

Clift, Grace & Weber (1978) derived empirical equations for the drag coefficient of spheres for higher Reynolds numbers. Their equation, valid for $Re < 800$,

$$c_D = \frac{24}{Re_d}(1 + 0.15 Re_d^{0.687}), \tag{13}$$

predicts drag coefficients of $c_D = 5.0$ for plastic particles and $c_D = 1.8$ for glass particles. This equation, however, does not consider free-stream turbulence. Uhlherr & Sinclair (1970) reported that mean drag might be increased or decreased by free-stream turbulence. For particle Reynolds numbers of $5 < Re_d < 700$ and velocity fluctuations of $0.05U_s < u' < 0.5U_s$, free-stream turbulence increased the mean drag. This is consistent with the measured drag coefficient for glass particles but disagrees with the measured drag coefficient of the plastic particles. Since the measured drag coefficients for both types of particles are the same, it is speculated that turbulence scales smaller than the particles modify the boundary layer to such an extent that the drag coefficient becomes independent of the particle Reynolds number.

The difference between the mean square velocities in figures 15 and 16 was used to estimate the relative velocities between the two phases. The following curve fits were obtained for the mean square velocities of plastic particles

$$(v_p')^2 = 0.25\{(v_f')^2\}^{0.83}, \tag{14}$$

and glass particles

$$(v_p')^2 = 0.12\{(v_f')^2\}^{0.76}. \tag{15}$$

The computed drag coefficients and the differences in the velocity fluctuations of the phases will be used to estimate the additional energy dissipation.

5.2. *Turbulence field*

The decay curves in figures 19 and 20 show an increase in the dissipation rate as particles are added to the flow. The increase in the energy dissipation appears to be nearly proportional to the particle concentration. This implies that the interaction of the individual particles with the fluid is independent of the concentration levels considered. This is consistent with the facts that the shape of the boundary layers of

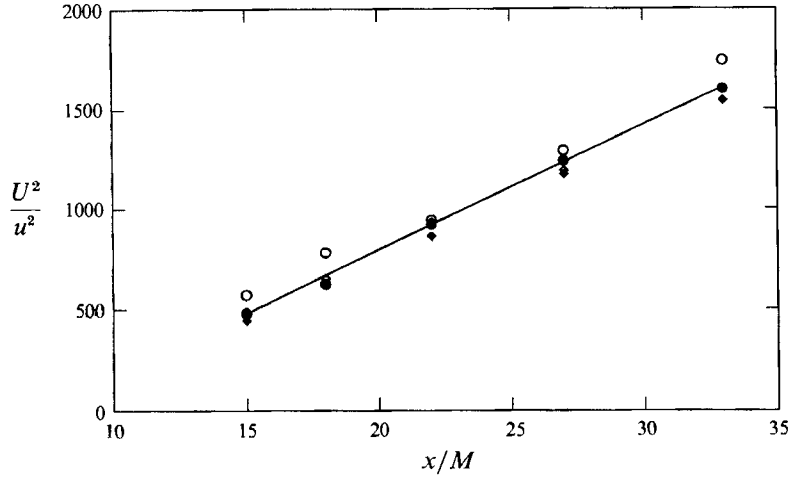

FIGURE 29. Predicted decay curve for the liquid phase in a suspension of 1% of plastic particles from data in figure 19. —, curve fit; ○, $C = 0.4\%$; ●, $C = 0.8\%$; ◇, $C = 1.2\%$; ◆, $C = 1.5\%$.

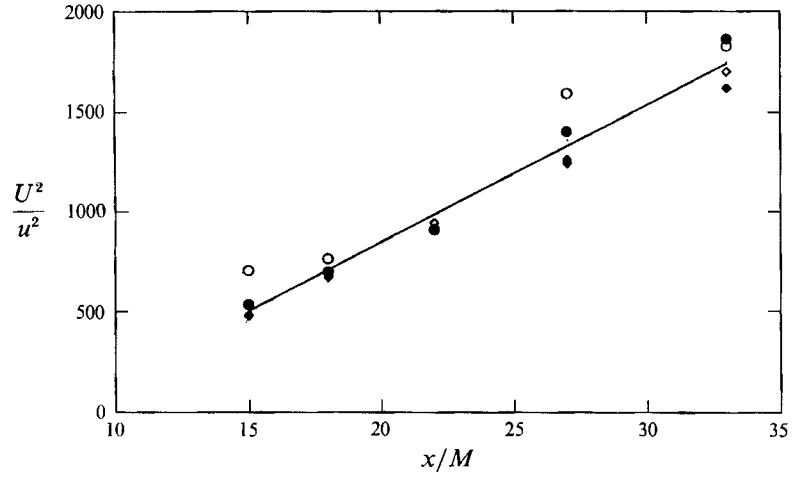

FIGURE 30. Predicted decay curve for the liquid phase in a suspension of 1% concentration glass particles from data in figure 20. —, curve fit; ○, $C = 0.4\%$; ●, $C = 0.8\%$; ◇, $C = 1.2\%$; ◆, $C = 1.5\%$.

the particles, the settling velocities, and the particle velocity fluctuations do not change with concentration. With the assumption of linearity, decay curves for volume concentrations of 1% were predicted from the individual decay curves. The results are presented in figures 29 and 30. The turbulence intensities of the suspensions follow a similar decay law to that of the single-phase flow. Applying a linear decay law to the data the following relationships were obtained for the liquid phase in suspensions of plastic particles

$$\frac{U^2}{u^2} = 61.2\left[\frac{x}{M} - 7.8\right], \tag{16}$$

and glass particles,

$$\frac{U^2}{u^2} = 68.9\left[\frac{x}{M} - 7.7\right]. \tag{17}$$

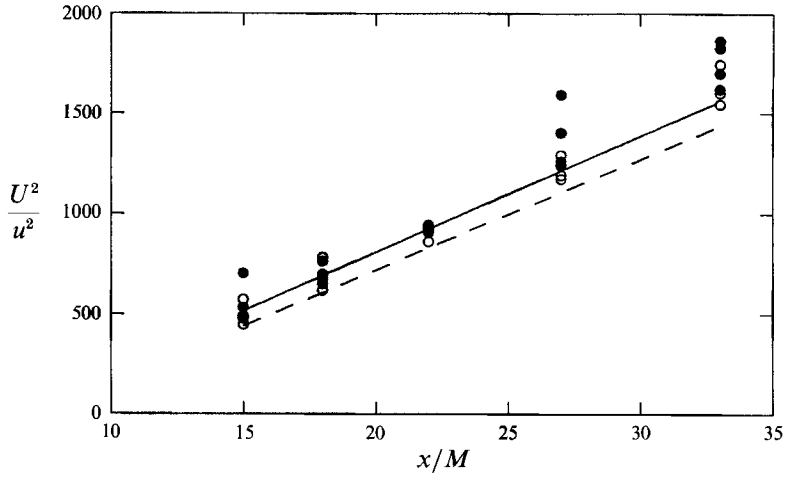

FIGURE 31. Computed decay curves for the liquid phase in suspensions of 1% concentration of particles. The additional dissipation is predicted by (18). ●, particles; ---, predicted by (20); ●, glass particles; —, predicted by (20).

The linear decay laws are indicated by solid lines in figure 29 and 30. For volume concentrations of 1%, the decay of turbulence energy is increased by about 17% by plastic particles and about 31% by glass particles.

A simple model of the frictional losses due to the relative motion between the phases was used to predict the increase in the dissipation of the turbulence energy. The additional dissipation of turbulence energy is predicted by:

$$\frac{\mathrm{d}}{\mathrm{d}t}E = F_{\mathrm{D}}\,\Delta v' N = \left(c_{\mathrm{d}\frac{1}{2}}\rho_{\mathrm{f}}(\Delta v')^2\pi\frac{d_{\mathrm{p}}}{4}\right)\Delta v' N, \tag{18}$$

where F_{D} is the average drag force on a particle, $\Delta v'$ is the relative velocity between the phases, and N is the number of particles. With

$$(\Delta v')^2 = (v_{\mathrm{f}}')^2 - (v_{\mathrm{p}}')^2, \tag{19}$$

the magnitude of the relative velocity Δv is estimated from (14) and (15). The additional energy dissipation is then computed from (18). The resulting decay curves are shown in figure 31. The model underestimates the additional dissipation due to the presence of particles. The predicted increase of the dissipation rate is about 4.4% and 9.4% for 1.0 volume per cent of plastic and glass particles, respectively.

The simple model does not completely account for the observed increase in the dissipation of turbulence energy. The model neglects possible changes in the dissipation rate due to the modification of the spectral distribution of the turbulence energy. As shown, sufficiently high concentrations of particles alter the high wavenumber end of the energy spectra and, thus, the energy dissipation. Tsuji *et al.* (1984) experimentally investigated a particle-laden pipe flow. Energy spectra of the streamwise velocity component of the airflow were estimated from LDV measurements. Large plastic particles (1.0 and 3.0 mm) did not modify the energy spectra across the pipe diameter. Small particles (0.2 and 0.5 mm) increased the energy at high wavenumber in the core of the pipe flow. This is in agreement with the current study, i.e. particles of large inertia do not change the streamwise energy spectra, whereas particles of smaller inertia increase the energy at high wavenumbers. However, it is also observed that the

transverse energy spectra are reduced at high wavenumbers. Both effects are consistent with an increase in the isotropy of the flow field as illustrated in figures 25 and 26. The inhomogeneity and anisotropy of pipe flows might explain why Tsuji *et al.* found a variation of the effect of small particles on the streamwise energy spectra across the pipe.

Hetsroni & Sokolov (1971) measured the streamwise velocity spectra in a droplet-laden jet flow. They observed a monotonic decrease of the energy at high wavenumbers with particle concentration. This is in contrast to the measurements by Tsuji *et al.* and the present work. Hetsroni & Sokolov measured the gas velocity with a standard hotwire. Droplets impinging on the wire caused spikes in the time trace of the velocity signal. These spikes were removed by clipping. Since clipping is equivalent to a low-pass filter, it is not certain to what extent the decrease of the turbulence energy at high wavenumbers is due to data processing of the recorded signals.

As has been shown, solid particles can have opposite effects on the individual components of the velocity fluctuations. Thus, spectral information of all velocity components is necessary to estimate the effect of particles on the total energy spectrum. The one-dimensional spectra in figures 27 and 38 suggest that the energy at low wavenumbers is not effected by the presence of particles. The energy at high wavenumbers, however, is slightly decreased by glass particles. Since the dissipation rate $D(k)$ is related to the turbulence energy $E(k)$ by

$$D(k) = 2\nu k^2 E(k), \tag{20}$$

changes in turbulence energy at high wavenumbers also affect the energy dissipation. The measured energy spectra (figures 27 and 28) suggest that energy dissipation due to fluid–fluid interactions is decreased by glass particles. This is not consistent with the measured increase in the dissipation rate in the presence of glass particles (figures 19 and 20). Also, this conclusion is speculative, since the high wavenumber end of the spectra which contributes most to the energy dissipation could not be properly resolved. A decrease of the dissipation rate by heavy particles was predicted by Hetsroni & Sokolov (1971) using the same line of arguments, i.e. particles decrease the energy at high wavenumbers and therefore decrease the dissipation of turbulence energy. Their prediction, however, is not supported by the measured decay curves. Baw & Penskin (1971) also predicted a decrease in the energy density at high wavenumbers, which would consequently result in a reduced dissipation rate. In their derivation, however, they state that effects of the solid phase on third- and higher-order velocity correlations is assumed to be negligible. However, third-order velocity correlations are associated with the transfer of energy across the wavenumber spectrum and might play an important role in the modification of the energy content at high wavenumbers. A possible explanation for the observed increase in dissipation rate is given by Derevich (1987). He argues that particles might alter the energy transfer from large eddies to smaller eddies. Derevich predicts that particles of moderate inertia increase the transfer of energy to smaller scales extending the energy spectrum to higher wavenumbers. Since the transfer of energy at wavenumber k equals the dissipation at wavenumbers larger than k, an increase in the energy transfer is associated with an increase in the dissipation rate.

The observed increase in the isotropy indicates that particles enhance the exchange of momentum from one velocity component to the other. It is quite possible that the transfer of energy to smaller eddies is also increased, since both mechanisms are based on vortex interaction. An attempt was made to estimate the transfer spectra from triple velocity correlations. However, the inherent noise of LDV signals and the poor

convergence of triple correlations (Uberoi 1963; Van Atta & Chen 1968) made reasonable estimates of the transfer function impossible.

6. Summary and conclusions

The effects of solid particles on the decaying turbulence field downstream of a grid were investigated experimentally. Particles with an average size of 655 μm and densities of 1050 kg/m^3 and 2400 kg/m^3 were used in a water flow facility. Mean velocity and velocity fluctuations of both phases were measured by a laser-Doppler velocimeter. From the velocities of the liquid phase, decay curves and energy spectra were estimated.

It was found the drag coefficient of the particles was modified by the free-stream turbulence. The calculated drag coefficients for both types of particles were equal and constant. It is speculated that the small turbulence scales modify the boundary layers of the particles to the extent that the drag coefficient becomes independent of the particle Reynolds numbers. Measured transverse velocity fluctuations of both phases indicate that the particles do not completely follow the velocity fluctuations of the liquid phase. The ratio of the velocity fluctuations of the particles to that of the fluid increases with increasing turbulence intensity.

The presence of particles in sufficiently high concentrations modified the turbulence field downstream of the grid. The decay rate of the turbulence energy increased monotonically with particle concentration. The additional dissipation rate for the suspensions of heavier glass particles was about double that of the almost neutrally buoyant plastic particles. The decay curves of the suspensions followed a linear decay law similar to that of the single-phase flow. A simple model based on the slip velocity between the phases under-predicted the measured increase in the dissipation rate. A large portion of the additional dissipation rate is probably associated with the modification of the spectral distribution of the turbulence energy. Measured longitudinal and transverse energy spectra show an increase in the isotropy of the flow field in the presence of particles. The increased isotropy of suspensions indicates that fluid–fluid interaction, the basic mechanism of energy transfer, is enhanced in the presents of particles. An increased energy transfer also results in a decrease of the Kolmogorov microscale and an increase in the dissipation rate.

REFERENCES

AL TAWEEL, A. M. & LANDAU, J. 1977 Turbulence modulation in two-phase jets. *Intl J. Multiphase Flow* **3**, 341.

BATCHELOR, G. K. & TOWNSEND, A. A. 1949 Decay of isotropic turbulence in the initial period. *Proc. R. Soc. Lond.* A **193**, 539.

BAW, P. S. H. & PESKIN, R. L. 1971 Some aspects of gas–solid suspension turbulence. *Trans ASME* D: *J. Basic Engng* p. 631.

BUCHHAVE, P. 1978 The measurement of turbulence with the burst-type laser Doppler anemometer – errors and correction methods. Ph.D. dissertation, State University of New York, Buffalo.

BUCHHAVE, P. & GEORGE, W. K. 1979 Bias correction in turbulence measurements by the laser Doppler anemometer. In *Laser Velocimetry and Particle Sizing* (ed. H. D. Thompson & W. H. Stevenson). Hemisphere.

CLIFT, R., GRACE, J. R. & WEBER, M. E. 1978 *Bubbles, Drops and Particles.* Academic.

COMTE-BELLOT, G. V. & CORRSIN, S. 1966 The use of a contraction to improve the isotropy of grid-generated turbulence. *J. Fluid Mech.* **25**, 657.

DEREVICH, I. V. 1987 The velocity fluctuation spectrum of a gas with particles in the case of uniform isotropic turbulence. *Fluid Dyn.* **22** (1) (Translation from *Izv. Akad. Nauk SSSR Mech. Zhid. i Gaza*, no. 1, p. 59, 1987).

HETSRONI, G. & SOKOLOV, M. 1971 Distribution of mass, velocity, and intensity of turbulence in a two-phase turbulent jet. *Trans ASME* E: *J. Appl. Mech.* **38**, 315.

HINZE, J. O. 1975 *Turbulence*. McGraw-Hill.

LEE, S. L. 1987 Particle drag in a dilute turbulent two-phase suspension flow. *Intl J. Multiphase Flow*, **13** (2), 247–256.

MCLAUGHLIN, D. K. & TIEDERMAN, W. G. 1973 Biasing correction for individual realization of laser anemometer measurements in turbulent flows. *Phys. Fluids* **16**, 2082.

TENNEKES, H. & LUMLEY, J. L. 1972 *A First Course in Turbulence*. MIT Press.

TSUJI, Y., MORIKAWA, Y. & SHIOMI, H. H. 1984 LDV measurements of an air–solid two-phase flow in a vertical pipe. *J. Fluid Mech.* **139**, 417

UBEROI, M. S. 1963 Energy transfer in isotropic turbulence. *Phys. Fluids* **6** (8), 1048.

UHLHERR, P. H. T. & SINCLAIR, C. G. 1970 *Proc. Chemeca '70*, vol. 1, p. 1. Melbourne: Butterworths.

VAN ATTA, C. W. & CHEN, W. Y. 1968 Correlation measurements in grid turbulence using digital harmonic analysis. *J. Fluid Mech.* **34**, 497.

VAN ATTA, C. W. & CHEN, W. Y. 1970 Measurements of spectral energy transfer in grid turbulence. *J. Fluid Mech.* **38**, 743.